Physical Modelling in Geotechnics

Physical modelling of multiphase interaction problems in marine sediment

B. Zhu, L. Wang, D.Q. Kong & Y. Chen
College of Civil Engineering and Architecture, Zhejiang University, China

ABSTRACT: Offshore geotechnical engineering is typically associated with multiphase interaction problems, which to a large extent is dominated by the gravitational field. Tests conducted under centrifugal hypergravity are capable of reproducing the stress field of the prototype in laboratory, thus enabling effective modelling of multiphase interactions at very large scale. This study summarizes the noninertial frame effect of hypergravity experiments, and presents some typical hypergravity tests of offshore engineering. The similitude of hypergravity experiments in multiphase marine sediment are discussed for solid-liquid interaction and solid-liquid-gas-thermal coupling effect. Effect of loading rate on lateral behaviour of monopiles in saturated sand was examined first, in terms of the mechanical behaviour of the pile and the development of excess pore pressure around it. Then the hypergravity effects on thermo-hydro-mechanical behaviour of saturated soils is evaluated. The existence of gas would introduce evaporation/condensation of the liquid, compression / expansion of the gas and the liquid-gas seepage, etc. into the soil behaviour. When hydrate exists, the dissociation of hydrates via various processes such as free gas generation, gas and water migration as well as sediment softening further complicate such problems. Following the discussions of these issues, the comparison of hydrate dissociation in hyper- and normal-gravity model tests by depressurization is presented to highlight the advantage of hyper-gravity experiments in modelling multi-phrase problems in marine sediments.

Keywords: multiphase, hypergravity, marine sediment, scaling law, monopiles, hydrate

1 INTRODUCTION

The mechanical behaviour of marine sediments is typically associated with multiphase interaction, which is widely reported to have strong effects on the stiffness and strength of the sediment and as a result impose great threaten to practical engineering applications. For offshore foundations, e.g. wind turbines / drilling platforms (Zhu et al., 2018), great excess pore pressure (EPP) would accumulate at the presence of waves or storms, which accordingly cause remarkable decrease in the effective stress. During the dissipation of EPP, pore fluid flow and possible sand migration will be induced for hydraulic gradient, which may induce large skeleton deformation in marine sediment. For the non-isothermal applications, e.g. heated pipelines for oil / gas transportation (Zhu et al., 2020) or wells for gas hydrate exploitation (Zhou et al., 2021), gas generation and thermal expansion both for pore gas and liquid may occur, bringing more complicated processes. The effective stress, increasing with depth on account of gravity, plays a crucial role in the mechanical behaviour of marine sediment skeleton. Furthermore, these applications usually involve tens or even hundreds of meters in scale for marine sediment. The multiphase interaction in marine sediment brings a great challenge for physical simulation.

1g-model (Yavari et al., 2016) and centrifuge model (Ng et al., 2014) tests are the effective means to study the aforesaid multiphase interaction problems in marine sediment. Although 1g-model tests meet the demands in some cases, scaled centrifuge tests can precisely reflect the prototypes highly related to gravity, especially for soil consolidations and stress-related processes (Taylor, 2018). By developing a series of inflight devices for hypergravity experiments, researchers worldwide have obtained scientific breakthroughs and created engineering applications.

2 NONINERTIAL FRAME EFFECT OF CENTRIFUGAL HYPERGRAVITY

Figure 1 shows the Centrifugal acceleration and effective payload of some high-performance centrifuges in the world. Centrifuges have been widely used in the research of geotechnical and geological fields. The high-speed rotation of the centrifuge beam produces centrifugal acceleration in the gondola; the magnitude and direction of the centrifugal force vary with the rotation radius, exhibiting the nonlinear distribution. the rotating coordinate system of the centrifuge is a noninertial reference frame, and the matter motion in the chamber is subjected to convected inertial force and Coriolis inertial force. The noninertial frame effect, which is a coupling effect of the linearly-distributed centrifugal force, nonlinearly-distributed centrifugal force, and Coriolis force, can be used to evaluate centrifugal hypergravity quantitatively.

The influence of the nonlinearly-distributed centrifugal force on the hypergravity field can be evaluated by the ratio λ_1 between the nonlinearly-distributed centrifugal force to hypergravity (Chen et al., 2022):

$$\lambda_1 = \frac{a_u}{Ng} = \frac{h}{\sqrt{2}R_0} \quad (1)$$

where $a_u = h\Omega^2/\sqrt{2}$, h is the size of the experimental chamber and Ω is the angular velocity vector of the centrifuge rotation; R_0 is the rotation radius vector of the centrifuge beam.

The influence of the Coriolis force can be quantitatively evaluated by the ratio λ_2 between the Coriolis force and hypergravity (Chen et al., 2022):

$$\lambda_2 = \frac{a_c}{Ng} = \frac{2v'}{\sqrt{R_0 Ng}} \quad (2)$$

where v' is the substance's velocity in the coordinate system of hypergravity model.

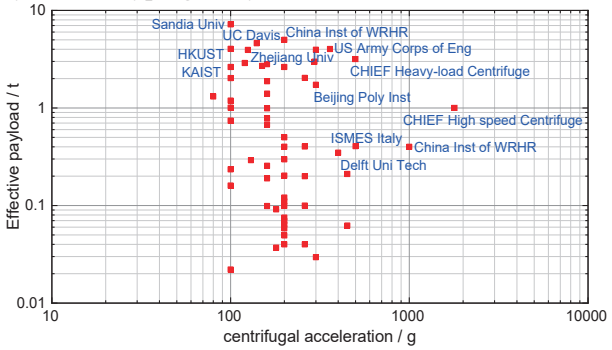

Fig. 1 Centrifugal acceleration and effective payload of some high-performance centrifuges in the world.

The evaluation of the linearity of the centrifugal hypergravity distribution is shown in Fig. 2. For the same model size, λ_1 gradually decreases as the centrifuge beam length increases. The allowable λ_1 given by (Taylor, 1995) is around 17.5%. Most centrifuges, such as the ZJU400, have a centrifugal acceleration deviation of less than 15%. Fig. 2 shows that the linearity of the hypergravity field created by the same centrifuge beam length decreases with an increase in the size of the experimental chamber. Therefore, the linearity of the hypergravity field in a large experimental chamber can be improved by increasing the length of the centrifuge beam. Eq. (2) indicates that the Coriolis force is related to the substance's velocity, the length of the centrifuge beam, and the centrifuge acceleration. According to (Schofield, 1980), the Coriolis force should be less than about 1.6% of ideal hypergravity. As shown in Fig. 3, the influence of the Coriolis force can be ignored if N is larger than 300 with R_0=5 m and v' about 1 m/s; however, if N is less than 300, this effect cannot be ignored. At this time, the effect of the Coriolis force can be reduced by increasing the length of the centrifuge beam and decreasing the substance's velocity.

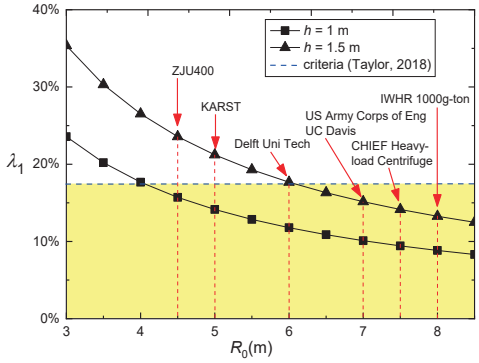

Fig. 2 Effect of the nonhomogeneous centrifugal hypergravity

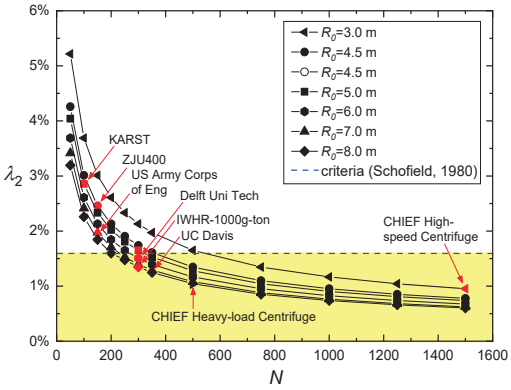

Fig. 3 Effect of the Coriolis force

3 USING SEEPAGE SIMIARITY FOR STUDYING LATERAL BEHAVIOUR OF MONOPILES IN SATURATED SOILS

This section presents a program of centrifuge tests on the lateral behaviour of monopoles (Kong et al., 2021). The diameter of the model pile was 0.059 m and the acceleration level of the tests was 100g. In addition to the routine measurements such as lateral load-displacement response, the net soil pressures acting on the pile and excess pore pressure around it was monitored as well.

The Scaling factors of this series of tests was summarized in Table 1. Silicon oil with viscosity of 100 times that of water was used, in order to satisfy the time-scaling requirement.

Table 1. Scaling factors adopted in pile loading tests in sand

Classification	Property	Model/Prototype
Geometric dimension	Length	1:n
Material property	Unit weight	n:1
	Rigidity stiffness	1:n^4
	Weight	1:n^3
External conditions	Velocity	1:1
	Concentrated load	1:n^2
Characteristics	Stress	1:1
	Strain	1:1
	Displacement	1:n
	Consolidation	1:n^2

Note: n is the centrifugal acceleration.

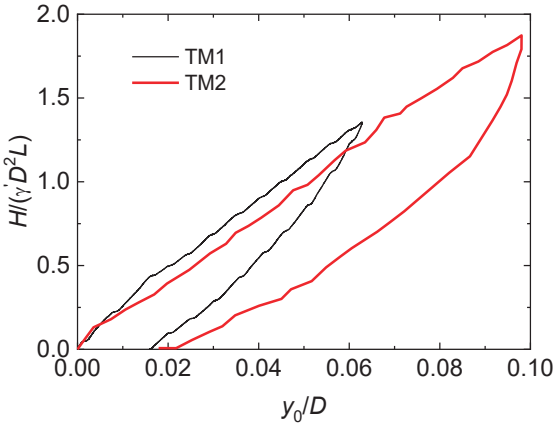

Fig. 4 Load-displacement curves during monotonic loading

Figure 4 shows the normalized load-displacement curves of the tests. Here H is the lateral load, L is the embedment depth, and D is the pile diameter. Both curves, at the loading stage, show characteristic of soil hardening with the increase of y_0, without any yielding behavior. The fast loading case TM2 (20 mm/s) surprisingly show a softer response than the slow loading case TM1 (0.01 mm/s), and this will be further explored in terms of *p-y* curves and the excess pore pressure development later (Kong et al., 2021).

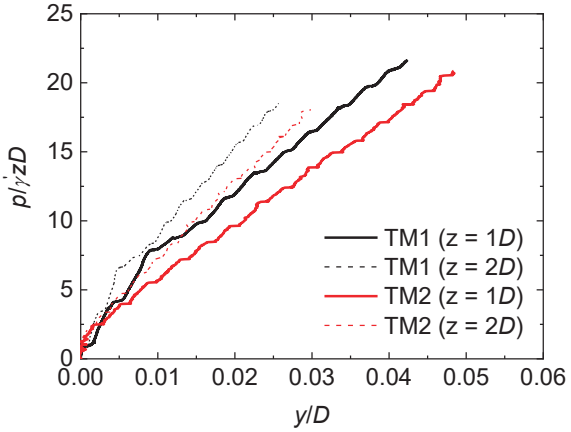

Fig. 5 p–y curves of TM1 and TM2 at different depth

Figure 5 compares the *p–y* curves obtained at the depths of 1D and 2D for the two tests. The fully drained case is associated with stronger *p-y* response than the partially drained one, confirming the weakening effect of loading rate on pile–soil interaction in sand, and all *p–y* curves show very good linearity. The ultimate state in traditional API *p–y* curve for small diameter piles cannot be reached for the cases examined here. This is also in consistence with the hardening load-displacement behavior observed in Fig. 4.

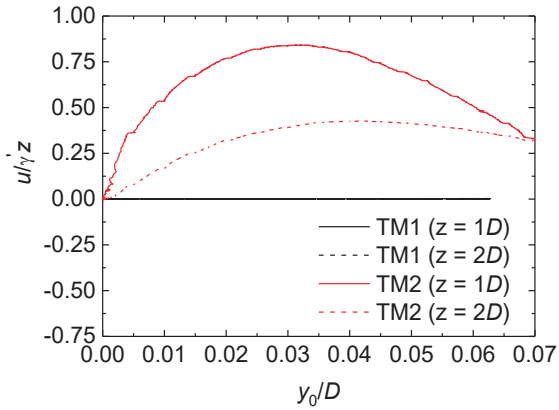

Fig. 6 Development of excess pore pressure (pile front) against the lateral pile deflection

Figure 6 plots the EPP (u) against the lateral pile deflection at mudline (y_0). The data was collected from EPP transducers installed at the depths of 1D and 2D in front of the pile. TM1 is clearly a drained test since very limited u can be seen. In contrast, notable development of excess pore pressure can be seen in TM2, showing an accumulation stage followed by a dissipation one. This may suggest a gradual establishment of a dominant seepage path (Zhu et al., 2021(b)).

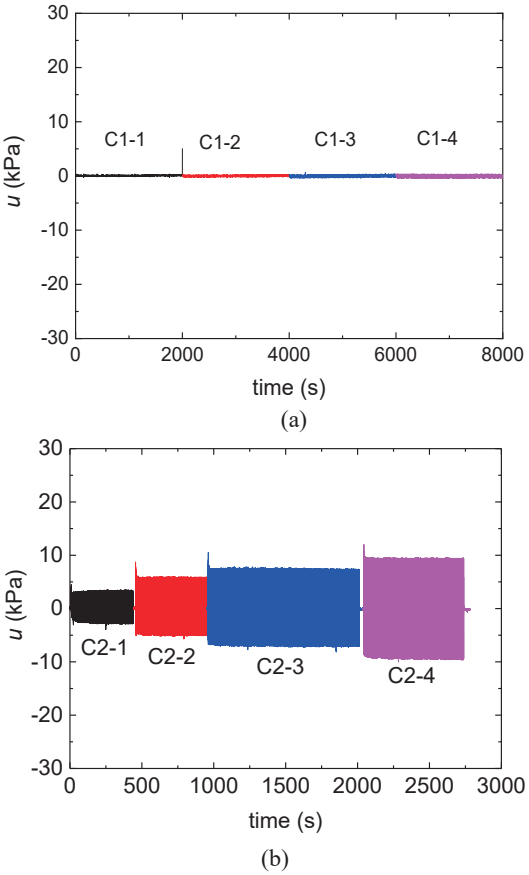

Fig. 7 Time trace of excess pore pressure at z = 1D: (a) TC1, (b) TC2

Figure 7 compares the time trace of EPP at z = 1D for two cyclic tests, termed TC1 (f = 0.05 Hz) and TC2 (f = 5 Hz). The observation in TC1 implies that for wave loadings with frequency lower than 0.05 Hz (e.g. infra-gravity waves and long-period waves), it may be reasonable to ignore the EPP accumulation when assess the pile-soil interaction for monopiles in sand (Kong et al., 2021). Though there is clear oscillatory EPP in TC2, with the amplitude strongly dependent on the cyclic load amplitude, accumulation of EPP is absent. This observation, together with that for monotonic loading, may possibly indicate that loading rate only has discernible effect on monotonic loading and the initial stage of cyclic loading. Of interest to note is that, despite the one-way feature of the cyclic load, the loading and unloading cycles are associated with a two-sided pattern of EPP development.

4 SIMILARITY OF HYPERGRAVITY EXPERIMENTS IN MULTIPHASE MARINE SEDIMENT

4.1 Hypergravity effects in saturated sediment

Centrifuge tests are of great convenient and inexpensive for reflecting the practical engineering, where scale factors of parameters are determined based on scaling laws, including dimensional analysis (Schofield, 1980) and governing equation analysis (Nahavandi et al., 1979). Derived from governing equations, e.g. mass balance / energy conservation equation, and constitutive relationships, e.g. Darcy's / Fourier's law in saturated sediment (Zhu et al., 2021(a) and 2021(d)), the scale factors for constant parameters for non-isothermal consolidation problems in saturated sediments are summarized in Table 2, are required during experiment to satisfy the similarity.

Table 2. Centrifuge modelling similarity rate for non-isothermal saturated sediment.

Classification	Property/parameter	Model/Prototype
Geometric dimension	Length	1:n
Duration	Time	1:n^2
Mechanics	Total / effective stress	1:1
	Strain	1:1
	Displacement	1:n
	Elasticity	1:1
	Poisson's ratio	1:1
Liquid flow	Pressure	1:1
	Viscosity	1:1
	Permeability	1:1
	Velocity	n:1
Heat transfer	Thermal expansion coefficient	1:1
	Specific heat capacity	1:1
	Heat conduction coefficient	1:1
Others	Density	1:1
	Porosity	1:1

However, parameters in most cases are non-constant, such as the dependence of density on temperature and effective stresses. Generally, the scaling factor of a certain non-constant parameter can be expressed as:

$$\pi_{\text{rear}} = \frac{f\left(a_{1\text{m}},\ ...,\ a_{i\text{m}},\ b_{1\text{m}},\ ...,\ \text{b}_{j\text{m}}\right)}{f\left(a_{1\text{p}},\ ...,\ a_{i\text{p}},\ b_{1\text{p}},\ ...,\ \text{b}_{j\text{p}}\right)}\pi_{\text{r}} \tag{3}$$

where π represents the non-constant parameter, π_r is the scale factor of π when derived from scaling laws, and $f(a_1,..., a_i, b_1,..., b_j)$ is a function introduced to reflect the impacts of other parameters / variables on π.; b_j is the parameter / variable with its scaling factor equaling to *1*, such as *l*, *p* or others; a_i is the parameter / variable with its scaling factor not equaling to *1*, like *t*, *u* or others; and the subscript i and j respectively represent the total numbers for parameter groups a and b.

To satisfy the similarity, we should have $\pi_{rear} = \pi_r$. For parameters only affected by b_j, there exists $b_{jm} = b_{jp}$, meaning that $\pi_{rear} = \pi_r$ is true and no impact will be caused on the scaling factor of π, such as fluid viscosity affected by temperature and skeleton stiffness / strength affected by stress. As for parameters influenced by a_i, detailed analysis should be carried out to judge the correctness of $\pi_{rear} = \pi_r$ for $a_{im} \neq a_{ip}$. The typical parameter is porosity in the time-dependent degradable porous media, such as municipal solid waste, where porosity is related to *t*. Thus, Eq. (3) can be used to evaluate whether the similarity of centrifuge tests is met when there exist parameter / variable related parameters.

Previous parametric scaling factors derived from the governing equations meet the requirements of centrifuge tests. However, boundary conditions of the modelling box are not always the same with the prototype, such as water surface remains stable in the prototype for automatic fluid influx / outflux in Fig. 8(b), but varies in centrifuge tests for the limited boxes in Fig. 8(c) when heated. Therefore, a one-dimensional model is established to simulate the prototype, where constant pore pressure and instantaneous temperature increase ΔT are applied on the top boundary (Ye et al., 2022).

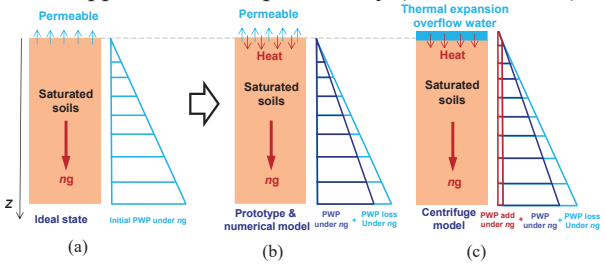

Fig. 8 Diagrams for thermal induced difference among ideal states, centrifuge and prototype / numerical model.

As the thermal expansion of pore water is much larger than that of soil particle, the theoretical

expressions for the pore water pressure (PWP) increase of prototype model and centrifuge model can respectively be expressed as:

$$\Delta p_{\mathrm{pro}} = -\int_0^z \rho_0^{\mathrm{w}} \beta_{\mathrm{w}} N g \Delta T(z)\,\mathrm{d}z \tag{4}$$

$$\Delta p_{\mathrm{cen}} = -\int_0^z \rho_0^{\mathrm{w}} \beta_{\mathrm{w}} N g \Delta T(z)\,\mathrm{d}z + \rho_0^{\mathrm{w}} (1-\beta_{\mathrm{w}} \Delta T) N g \Delta H \tag{5}$$

Accordingly, the steady-state PWP increase caused by temperature change for prototype and centrifuge models at any depth can be easily estimated, or the maximum values differentiating with ideal state are conveniently determined by model parameters. The PWP difference Δp is related with N, ΔT and φ in Fig. 9. For example, when H = 1.0 m, ng = 100, ΔT = 50 K and φ = 0.32, the maximum PWP increases of prototype and centrifuge models are separately 30.9 kPa and 21.0 kPa, and Δp is almost 10 kPa.

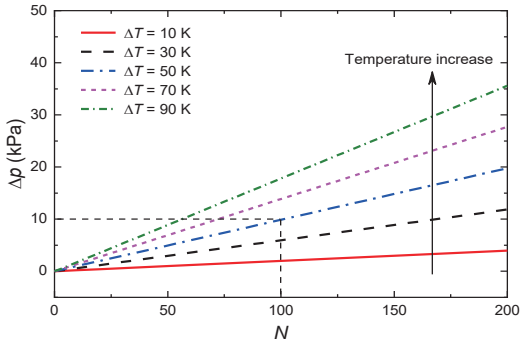

Fig. 9 PWP increment with different surface temperature change.

As is described above, the similarity of THM coupled responses of saturated soil for centrifuge tests meets the requirement of non-constant parameters once the scale factors of them are related with parameters / variables equaling to 1. Thus, both reduced scale models with H_m = 1 m under N = 1, 10 and 100, and prototype / numerical models with H_p = 10, 100, 200 m are established and compared. It could be noticed that there is no difference in temperature and PWP increment between the reduced scale models and prototype / numerical models, reflecting in different line types in Fig. 10. Besides, peak points of the PWP increment are mainly caused by thermal expansion of pore water, which will then gradually dissipate with time.

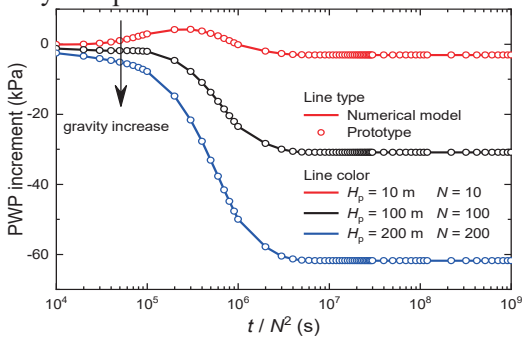

Fig. 10 Comparison of reduced scale and origin scale models on evolutions of PWP increment.

4.2 Solid-liquid-gas-thermal coupling effect in hydrate reservoir during gas production

For multiple interactions in unsaturated marine sediment, apart from the governing equations and constitutive relationships mentioned above, the air mass balance equation and equations of state for non-isothermal two-phase flow should be considered in unsaturated sediment (Zhu et al., 2020; Wang et al., 2022(a)). Similar to previous derivation according to scaling laws, the scale factors for key properties / parameters for non-isothermal two-phase flow in deformable sediment, summarized in Table 3, must be satisfied to meet the requirement for similarity in centrifuge modeling tests.

Table 3. Centrifuge modelling similarity rate for non-isothermal unsaturated sediment.

Classification	Property/parameter	Model/Prototype
Geometric dimension	Length	1:n
Duration	Time	1:n^2
Mechanics	Total / effective stress	1:1
	Displacement	1:n
Two-phase flow	Liquid / gas / capillary pressure	1:1
	Vapor pressure	1:1
	Diffusion coefficient	1:1
	Saturation	1:1
	Relative permeability	1:1
	Liquid / gas velocity	n:1
Heat transfer	Specific heat capacity	1:1
	Heat conduction coefficient	1:1

The multiphase interaction in unsaturated sediment consists of skeleton deformation, migration of pore water and air, heat transfer and phase transition of liquid water and vapor induced by temperature change is schematically depicted in Fig. 11 (Zhu et al., 2020). In detail, the pore liquid water evaporates for the soil temperature increment surrounding heated sources, which results in rising of gas pressure shown in Eqs. (6) and (7) and water vapor pressure shown in Eqs. (8) and (9) (Philip and De Vries, 1957; Wang et al., 2015; Zhu et al., 2020). Owing to the pressure gradient, water vapor diffuses outwards and then condenses to liquid water at lower temperature regions (Eqs. (8) and (9)), leading to decrease of local gas pressure (Eqs. (6) and (7)) (Zhu et al., 2020).

$$p_k^{\mathrm{g}} = \frac{\rho_k^{\mathrm{g}} R T}{M_k} \tag{6}$$

$$p^{\mathrm{g}} = p_{\mathrm{a}}^{\mathrm{g}} + p_{\mathrm{w}}^{\mathrm{g}} \tag{7}$$

$$p_{\mathrm{w}}^{\mathrm{g}} = p_{\mathrm{w\_sat}}^{\mathrm{g}} \exp\left(-\frac{p^{\mathrm{c}} M_{\mathrm{w}}}{\rho_{\mathrm{w}}^{\mathrm{l}} R T}\right) \tag{8}$$

$$p^{g}_{w\_sat} = 10^{-3}\frac{RT}{M_w}\exp\left(19.84 - \frac{4975.9}{T}\right) \quad (9)$$

where p_k^{π} is the partial pressure (subscript k ($k = w, a$) is the component and superscript π ($\pi = l, g$) represents the phase state), M_k is the molar mass, R is the ideal gas constant, and $p^{g}_{w\_sat}$ saturated vapor pressure.

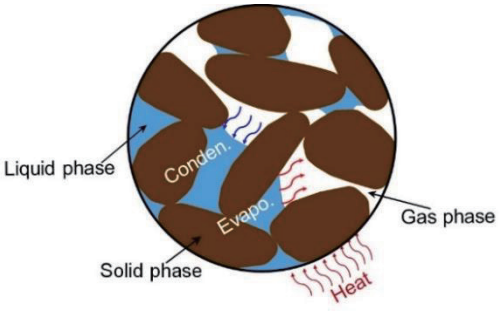

Fig. 11 Schematic of unsaturated sediment illustrating moisture evaporation and condensation

When hydrate exists, the dissociation of hydrates via various processes such as free gas generation, gas and water migration as well as sediment softening further complicate such problems. Wang et al. (2016) indicated that 27 dimensionless parameters should be consistent to satisfy the similarity between the tests and the gas production in the field reservoir. The normal gravity tests satisfy the consistency of 26 parameters except the gravity characterizing the stress distribution of the reservoir. It's essential to reproduce the stress gradient of field-scale hydrate reservoir for the mechanical behaviour and gas production characteristic during the hydrate exploitation, and the hypergravity test brings dawn to solve this problems.

Figure 12 shows the relative difference of PWP at different depths of the hydrate reservoir model at 40g and 100g. The PWP evolution is significantly affected by gravity during the hydrate dissociation. The pressure difference gradually increases as the gravity gradient, as well as the depth of the model, increases.

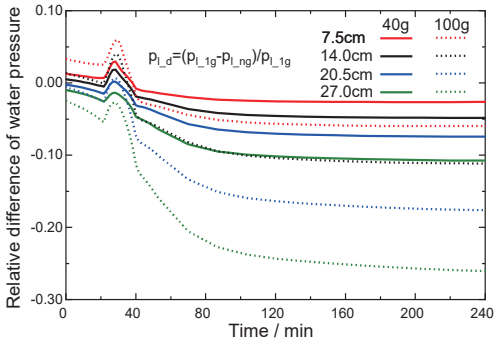

Fig. 12 Pressure difference during hydrate dissociation at 40g and 100g

Zhejiang university developed a hypergravity experimental apparatus to investigate the behaviour of hydrate sediments during gas production (Fig. 13) (Zhu et al., 2021(c); Wang et al.,2022(b)). The apparatus involves high-pressure vessel, pressure servo control unit, temperature control unit, hydrate synthesis unit, hydrate exploitation unit and monitoring unit, working normally at 100g. High pressure vessel is made of stainless steel 316L, whose bearing pressure is 20MPa. The inner effective volume of the vessel is 14.5L, with diameter of 230mm and height of 350mm. The core components of the apparatus were loaded on the centrifuge basket during the hypergravity test. The data acquisition system was installed in the center of the centrifuge. The other components were placed in the centrifuge power cabin and connected to the apparatus through pipelines (Wang et al., 2022(c)).

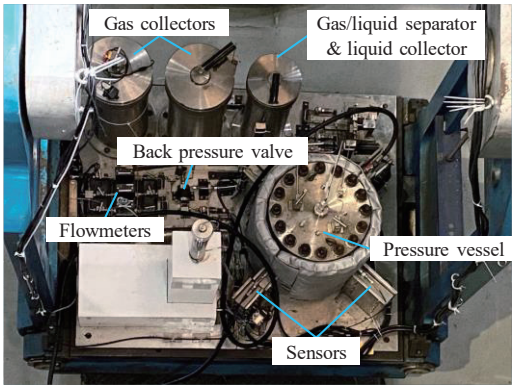

Fig. 13 the apparatus developed by Zhejiang University

In this test, a hydrate reservoir model with porosity of 0.445 and hydrate saturation of 0.24 was prepared and the acceleration level was 100g. The initial temperature and pressure of the model were 5℃ and 3.5 MPa respectively. Characteristic depressurizing rate of 0.05MPa/min was selected to drive hydrate dissociation at 1.5MPa.

Figure. 14 shows the evolution of EPP during hydrate dissociation. In the initial state, the exsolution gas and water formed hydrate due to depressurization, resulting in some pore seepage channels occupied additionally and confined lid formed. This process prevent the rate of depressurization and promote the accumulation of EPP. Then the dominant seepage channels formed due to the splitting of solid skeleton and the movement of fine particles during hydrate dissociation, leading to the rapid dissipation of excess pore pressure. The sediment skeleton at 100g showed higher strength and stiffness than that of at 1g case due to the influence of field-scale stress gradient.

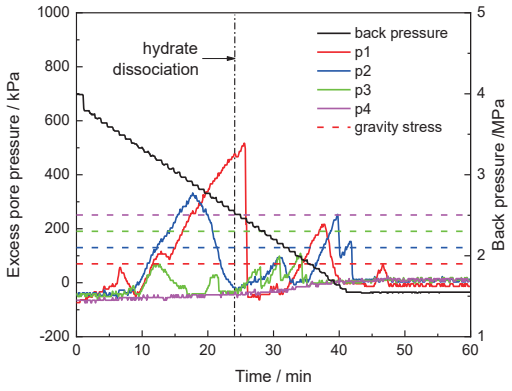

Fig. 14 Evolution of EPP during hydrate dissociation at 100g

Figure 15 compares the gas recovery ration during hydrate dissociation at 1g and 100g. Hypergravity increases the body force of matter, enhancing the driving force of the relative motion between substances with different densities and accelerating the evolution of multiphase media, consequently shortening the time required in the test. The complete dissociation of hydrate at 100g took less time than that in the 1g test, indicating that the hypergravity accelerated both the gas separation from hydrate and its migration to model surface. Furthermore, faster convective heat transfer at 100g improved the supplement efficiency of latent heat during hydrate dissociation.

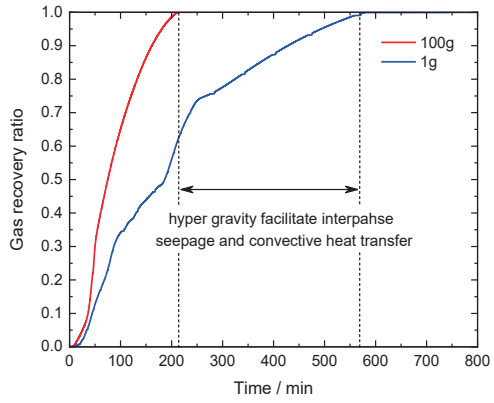

Fig. 15 Gas production during hydrate dissociation at 1g and 100g

5 CONCLUSIONS

This paper preliminarily discusses the similitude and centrifugal effect of hypergravity experiments. The model is subjected to nonuniform centrifugal acceleration and Coriolis forces, which inevitably cause experimental errors and undermine the similarity between the model and the prototype in multiphase and multi-field coupling interactions. In the case of pile loading behaviour in saturated sand, a linear relation between the lateral soil resistance and the pile deflection was observed, and the slope increased linearly with soil depth. The similarity for multiphase coupled centrifuge tests of saturated soil were derived based on governing equation analysis of scaling laws. For unsaturated soils, moisture evaporation and condensation can be caused by variations in temperature. Significant decrease in gas pressure and accordingly compression of soil can be induced by the thermally induced condensation of moisture, the extent of which exhibits strong positive correlation with the burial depth of the pipeline. When hydrate exists, hypergravity test is an effective approach to mimic the multi-phase interaction in marine sediments that can unconditionally achieve the consistency of scaling law between the model and prototype. Hydrate dissociation produced a large amount of gas, which made the excess pore pressure rise rapidly, drove the skeleton to split and form the dominant seepage channels. The gas production behavior between hyper- and normal-gravity model tests highlights the advantage of hyper-gravity experiments in modelling multi-phrase problems in marine sediments.

ACKNOWLEDGEMENTS

The authors acknowledge the funds from the National Natural Science Foundation of China (Nos. 52127815, 51988101 and 52078458).

REFERENCES

Chen, Y. M., Tang, Y., Ling D. S., Wang, Y. B. 2022. Hypergravity Experiments on Multiphase Media Evolution. Science China Technological Science. Doi: 10.1007/s11431-022-2125-x.

Ito, T., Komatsu, Y., Fujii, T., Suzuki, K., Egawa, K., Nakatsuka, Y. 2015. Lithological features of hydrate-bearing sediments and their relationship with gas hydrate saturation in the eastern Nankai Trough, Japan. Marine and Petroleum Geology. 66: 368-378.

Kong, D. Q., Zhu, J. S., Long, Y. W., Zhu, B., Yang, Q. J., Gao Y F and Chen, Y M. 2021. Centrifuge modelling on monotonic and cyclic lateral behavior of monopiles in kaolin clay. Géotechnique, 11: 1-14. Doi: https://doi.org/10.1680/jgeot.19.P.402.

Nahavandi, A. N. Castellana, F. S. & Moradkhanian, E. N. 1979. Scaling laws for modeling nuclear reactor systems. Nuclear Science and Engineering. 72(1): 75-83.

Ng, C.W.W. Shi, C. Gunawan, A. & Laloui, L. 2014. Centrifuge modelling of energy piles subjected to heating and cooling cycles in clay. Géotechnique letters, 4(4), 310-316. Géotechnique letters, 4(4): 310-316.

Philip, J. R. De Vries, D. A. 1957. Moisture movement in porous materials under temperature gradients. Eos, Transactions American Geophysical Union, 38(2): 222-232.

Schofield, A. N. 1980. Cambridge geotechnical centrifuge operations. Géotechnique. 30(3): 227-268.

Taylor, R.N. 1995. Geotechnical Centrifuge Technology. CRC Press.

Wang, L. J., Cleall, P., Zhu, B., Chen, Y.M., 2022(a). Modelling the thermal-hydro-mechanical behaviour of unsaturated soils with a high degree of saturation using extended precise integration method. Canadian Geotechnical Journal, DOI: 10.1139/cgj-2021-0201.

Wang, L. J., Wang, P., Wang, X. B., Zhu,B., Chen., Y. M. 2022(b).

Centrifuge modelling on behaviour of hydrate bearing sediments during gas production by depressurization. ICPMG, KAIST, Daejeon, Korea.

Wang, X. B., Wang, L. J., Zhu, B., Wang, P., Yuan, S. M., Chen, Y. M. 2022(c). Experimental study on the behavior of hydrate-bearing sediments during servo depressurization. Rock and Soil Mechanics. 43(9). Doi: 10.16285/j.rsm.2021.1956.

Wang, X. R., Shao, H., Wang, W. Q., Hesser, J., Kolditz, O. 2015. Numerical modeling of heating and hydration experiments on bentonite pellets. Engineering Geology, 198: 94-106.

Wang, Y., Feng, J. C., Li, X. S., Zhang, Y. 2016. Experimental and modeling analyses of scaling criteria for methane hydrate dissociation in sediment by depressurization. Applied Energy. 181: 299-309.

Yavari, N., Tang, A. M., Pereira, J. M., Hassen, G. 2016. Mechanical behaviour of a small-scale energy pile in saturated clay. Géotechnique. 66(11): 878-887.

Ye, Z. G., Zhu, B., Yuan, S. M., Wang, L. J., Chen., Y. M. 2022. Evaluation of hypergravity effects on thermo-hydro-mechanical behaviour of saturated soils. ICPMG, KAIST, Daejeon, Korea.

Zhu, B., Wen, K., Kong, D. Q., Zhu, Z. J., Wang L. J. 2018. A numerical study on the lateral loading behavior of offshore tetrapod piled jacket foundations in clay. Applied Ocean Research. 75: 165-177.

Zhu, B., Ye, Z. G., Wang, L. J., Kong, D. Q., Xu, W. J., Kolditz, O., Nagel, T., Chen, Y. M. 2020. Hydro-mechanical behavior of unsaturated soil surrounding a heated pipeline considering moisture evaporation and condensation. Computers and Geotechnics. 119: 103377.

Zhu, B., Huang, J. S., Wang, L. J., Ye, Z. G., 2021(a). Precise numerical study on the behaviour of gassy marine soils subjected to thermal and mechanical loadings. Computers and Geotechnics, 137, p.104269.

Zhu, B., Ren, J., Yuan, S. M., Zhu, J. S., Yang, Q. J., Gao, Y. F., Kong, D. Q. 2021(b). Centrifuge Modeling of Monotonic and Cyclic Lateral Behavior of Monopiles in Sand. Journal of Geotechnical and Geoenvironmental Engineering, ASCE. 147(8): 04021058.

Zhu, B., Wang, L. J., Yang, S. Q., Chen, Y. M., Kong, D. Q., Lin, W. A. 2021(c). Pressure-control temperature-control Hypergravity experimental device for simulating deep-sea seabed responses. U.S. Patent. US11,187,691 B2.

Zhu, B., Ye, Z. G., Wang, L. J., Xu, W. J., Kong, D., Nagel, T., Kolditz, O., Chen, Y. M., 2021(d). Theoretical investigation into thermo-osmosis and thermofiltration effects on hydromechanical behavior of saturated soils. Journal of Engineering Mechanics, 147(4): p.04021005.

Zhou, J. Z., Zhou, Y., Yang, Z. J., Wei, C. F., Wei, H. Z., Yan, R. T. 2021. Dissociation-Induced Deformation of Hydrate-Bearing Silty Sand During Depressurization Under Constant Effective Stress. Geophysical Research Letters. 48(14): e2021GL092860.